

Automatic Removal of Externally Attached Fiducial Markers in Cone Beam C-arm CT

Martin Berger^{1,2}, Christoph Forman^{1,3}, Chris Schwemmer^{1,3}, Jang H. Choi⁴,
Kerstin Müller^{1,3}, Andreas Maier¹, Joachim Hornegger¹, Rebecca Fahrig⁴

¹Pattern Recognition Lab, FAU Erlangen-Nürnberg

²Research Training Group 1773 “Heterogeneous Image Systems”

²Erlangen Graduate School in Advanced Optical Technologies (SAOT)

³Department of Radiology, Stanford University, Stanford, CA, USA

`martin.berger@cs.fau.de`

Abstract. In computed tomography fiducial markers are frequently used to obtain accurate point correspondences for further processing. These markers typically cause metal artefacts, decreasing image quality of the subsequent reconstruction and are therefore often removed from the projection data. The placement of such markers is usually done on a surface, separating two materials, e.g. skin and air. Hence, a correct restoration of the occluded area is difficult. In this work six state-of-the-art interpolation techniques for the removal of high-density fiducial markers from cone-beam CT projection data are compared. We conducted a qualitative and quantitative evaluation for the removal of such markers and the ability to reconstruct the adjoining edge. Results indicate that an iterative spectral deconvolution is best suited for this application, showing promising results in terms of edge, as well as noise restoration.

1 Introduction

A crucial step in medical image registration is to find accurate point correspondences, which can be clearly detected in all acquired images. In computed tomography (CT) fiducial markers, represented by small metallic beads, are often the method of choice. An advantage of fiducials is that they are well recognisable in the 2D projection images. However, after having exploited the markers’ spatial information, it is often necessary to remove them prior to further processing. One reason for this is that metallic markers typically lead to increased streaking artefacts in the reconstructed domain, substantially decreasing image quality. The position of the markers might also be used to provide ground truth information for further, marker-free processing methods [1].

Marker removal recovers missing data in the areas occluded by the object, using the known, surrounding pixel values. In CT reconstruction, various methods have been proposed to remove high-density objects from projection data. A simple but often adequate approach is to linearly interpolate the missing regions based on a specified neighbourhood. Additionally, spline-based techniques have

been proposed [1]. In contrast to spatial interpolation, an iterative spectral deconvolution approach has been introduced in [2], showing promising results on radiographic data. In [3], a concept has been proposed that also incorporates the hidden structural information underneath high-density objects.

Despite the multitude of available methods, little attention has been paid to the locational properties of the defects. Fiducial markers are usually attached externally at a distinct edge between two materials, e.g. skin and air. Accurately recovering this edge poses an additional challenge to the removal algorithm as many of them assume only low-frequency changes in a defect’s neighbourhood. In this work we compare the performance of six different algorithms for marker removal with a special focus on their ability to restore material edges.

2 Materials and Methods

2.1 Automatic Marker Detection

For marker detection we used a fully automatic pipeline based on the fast radial symmetry transform (FRST) [4]. Identifying corresponding markers over all projection images helps to reduce false positive detections. We solve this problem by an initial detection of the 3D marker positions. The algorithm works as follows:

1. Apply the FRST to all projection images $f_j(\mathbf{x})$, with $\mathbf{x} \in \mathbb{R}^2$ and $j \in [1, P]$.
2. Backproject a blurred version of the FRST outcome to 3D, yielding distinct blobs for each marker.
3. Binarise the blobs using the maximum entropy method [5] and apply a 3D connected component analysis. The components’ centroids then represent the 3D reference positions of each marker, denoted as $\mathbf{v}_i \in \mathbb{R}^3$ with $i \in [1, B]$. The number of markers B is given by the number of components.
4. Given the projection matrices \mathbf{P}_j , forward project the 3D reference points onto each projection image yielding the 2D reference points $\bar{\mathbf{u}}_{ij} = \mathbf{P}_j \mathbf{v}_i$, where j and i denote the j -th projection and i -th marker.
5. Extract a set of 2D candidate points \mathbf{u}_{ij} for each projection image from the initial FRST result, using a heuristically determined threshold and a 2D connected-components analysis.
6. Assign the candidate points to the closest 2D reference points, essentially solving the correspondence problem.

For a better accuracy, the 3D marker positions can be updated by the newly assigned candidate points and a method described in [6]. Thus, the algorithm can be applied iteratively by repeating step 4) to 6) with the updated 3D positions.

2.2 Marker Removal

As input for the marker removal we had the estimated 2D marker positions \mathbf{u}_{ij} , which were then used to extract a binary defect mask

$$w_j(\mathbf{x}) = \begin{cases} 0 & \text{if } \|\mathbf{x} - \mathbf{u}_{ij}\|_2 < r, \quad \forall i \in [1, B] \\ 1 & \text{otherwise} \end{cases}, \quad (1)$$

where r is derived from the marker size and determines the invalid area and $\|\cdot\|_2$ denotes the L2-norm. The removal was done separately for each marker using a square region centred at the marker’s position. Let us define the set

$$\Omega_{ij} = \{\mathbf{x} \mid \|\mathbf{x} - \mathbf{u}_{ij}\|_\infty < N/2\} \quad , \quad (2)$$

that includes all pixel locations that are part of the square region, where N is the region’s side length and $\|\cdot\|_\infty$ the infinity norm. Hence, the inputs for a removal method are given by $f_j(\mathbf{x}_\Omega)$ and $w_j(\mathbf{x}_\Omega)$, for all $\mathbf{x}_\Omega \in \Omega_{ij}$. Let us further define a subset of Ω_{ij} that contains all positions that are marked as defect, i.e.

$$\Gamma_{ij} = \{\mathbf{x} \mid \mathbf{x} \in \Omega_{ij} \wedge w_j(\mathbf{x}) = 0\} \quad . \quad (3)$$

Then the marker removal is described by estimating the missing data values at positions Γ_{ij} given the known data points at positions $(\Omega_{ij} \setminus \Gamma_{ij})$.

Six different interpolation techniques are compared. First we used a linear interpolation (LinInt) approach. Further we applied cubic B-splines (BSpl), estimated for each row and column separately [1]. The interpolation at the missing position \mathbf{x}_r is then computed by the mean of the corresponding row and column spline. We also used the more general thin-plate smoothing spline (TPSpl). Here a 2D surface is fitted to the valid pixels and evaluated at the missing positions. Normalised convolution (NConv) was applied as introduced in [7], which is a Gaussian low-pass filter, normalised by incorporating information from the given defect mask. We also applied the Subtract-and-Shift (SaS) method [3], which aims to recover remaining high-frequency structure from the occluded areas. Finally, the spectral defect interpolation (SpecInt) as proposed in [2] is applied. This method estimates the missing information by an iterative approach in the frequency domain, minimising the mean squared difference between the estimated and observed image over all positions in $(\Omega_{ij} \setminus \Gamma_{ij})$.

2.3 Data and Experiments

We had access to a C-arm CT scan of a left knee, containing 8 fiducial tantalum markers with 1 mm diameter, attached at distinct positions at the height of the patella. The data was acquired on an Axiom Artis dTA (Siemens AG, Forchheim, Germany), with a detector resolution of 1240×960 pixels, a pixel size of $0.308 \times 0.308 \text{ mm}^2$ and an angular resolution of 496 projections acquired over a range of 200° . Further we generated synthetic phantom projections, using the same geometry as for the real scan. The phantom consists of three encapsulated cylinders representing a simple model of tissue, bone and bone marrow. The cylinders have radii of 80 mm, 35 mm and 31.5 mm and their attenuation coefficients are set to water, bone and bone marrow, respectively. Eight metallic beads with 1 mm diameter are attached in a helical trajectory around the outer cylinder such that they overlap the cylinder’s surface by 0.1 mm. We also created marker free reference projections, to obtain ground truth data.

Each removal method was applied to all 8 markers over 496 projections yielding a total of 3968 interpolation steps per dataset and algorithm. Afterwards,

Table 1. Quantitative results for each marker removal method based on the synthetic dataset. The evaluated edge separates water (0 HU) and air (−1024 HU). “None” equals the reconstruction without marker removal.

	None	LinInt	BSpl	TPSpl	NConv	SaS	SpecInt
RMSE (HU)	30.12	13.84	9.26	9.91	19.50	14.62	8.08
σ_{rmse} (HU)	4.36	4.84	4.27	4.35	6.46	4.33	3.31

256×256×256 cubes were reconstructed centred at the bead positions, with a spacing of 0.125×0.125×0.125 mm³. We also reconstructed the non-corrected projections and the marker-less projections in the case of the synthetic data. For a quantitative comparison the root mean squared error (RMSE) between marker-free and interpolated reconstructions and its standard deviation over the different markers (σ_{rmse}) were computed. The methods’ parameters, e.g. the window width N , have been manually adjusted on the synthetic data.

3 Results

The quantitative results are shown in Tab. 1. Spectral interpolation performed best with an RMSE of 8.08 HU and a standard deviation of 3.31 HU. The spline-based approaches performed similarly well, followed by the linear interpolation and Subtract-and-Shift. The normalised convolution showed a substantially worse performance and also the highest standard deviation.

Fig. 1 depicts 16×16 mm² regions centred around each marker. The ground truth surface of the cylinder is overlaid as a dashed yellow line. Spectral interpolation shows the best result, almost perfectly recovering the cylinder’s edge. The spline-based approaches show similar results with a slightly more blurred edge. Increased blurring can be seen with linear interpolation and SaS, where the latter could not remove the marker completely. Normalised convolution produced streaking artefacts and could not sufficiently restore the missing information.

In Fig. 2 we show the results for the C-arm CT acquisitions, where Fig. 2a gives an overview of the full reconstruction. A considerable amount of noise was present which ideally would be restored in the defective area. The spectral interpolation approach performed best, yielding a distinct edge profile and also restoring the noise level. Compared to the synthetic data, the B-spline approach produced noticeable streaking artefacts, whereas the thin-plate-splines showed increased blurring making the outcome comparable to a linear interpolation. The SaS was not able to remove the marker completely, yet the edge was well restored and the noise level retained. The normalised convolution showed similar artefacts as for the simulated data and performed worst.

4 Discussion

The results show that the spectral interpolation approach accurately restores edges as well as noise properties. An important parameter for this algorithm is

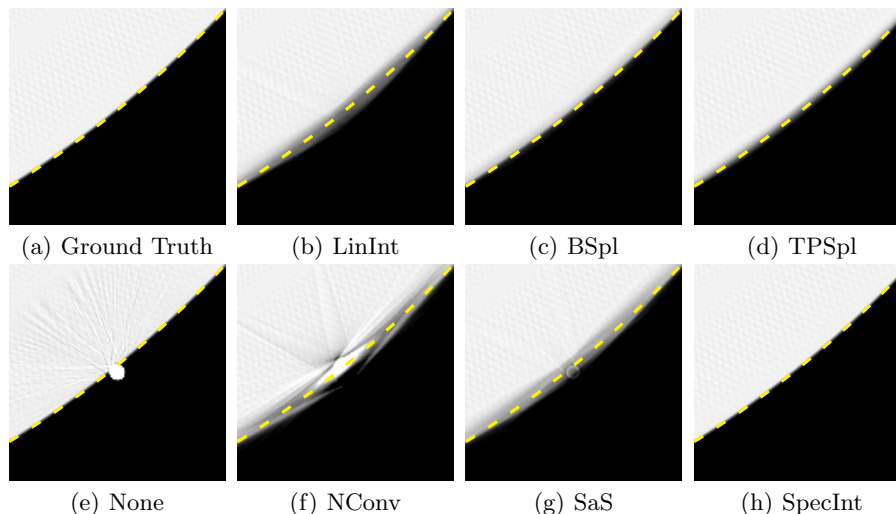


Fig. 1. Bead removal results for the synthetic dataset. The images show a $16 \times 16 \text{ mm}^2$ region centred around the marker. The display window was $[-922, 51]$ HU.

the location and width of the support region. In our data the markers' size was constant and their positions known, which might be one reason for the good performance. The spline-based approaches did not retain the high performance seen from the synthetic data when applied to the real data. The B-Spline approach showed increased streaking artefacts which might be due to the increased noise level of the real data. This seems reasonable as values are determined by information based on the line and column only, not involving any other neighbourhood. The thin-plate-spline shows an increased smoothing effect on real data, which might be due to an additional increase in the regularisation parameter needed to cope with the noise level. Simple linear interpolation robustly removes markers but tends to smooth the adjoining edge. By definition the SaS method aims to retain high-frequency information, which is then aligned with the surrounding intensities [3]. The method was not able to remove the markers completely, which we think is due to the high frequency implied by the small markers itself. No sufficient performance was obtained when using the normalised convolution which does not seem to be suitable for marker removal on surfaces.

We compared six techniques for the removal of high-density fiducial markers from cone-beam CT projection data. The placement of the markers is typically done on a distinct surface, which makes a correct restoration of the 3D reconstruction more difficult. This study shows a qualitative and quantitative comparison for the removal of such markers and the ability to reconstruct the adjoining material edge. The results show that the spectral interpolation approach is best suited for our application, showing promising results in terms of edge, as well as noise restoration. An extension of this evaluation to arbitrary shaped markers as well as data with patient-motion will be the subject of future work.

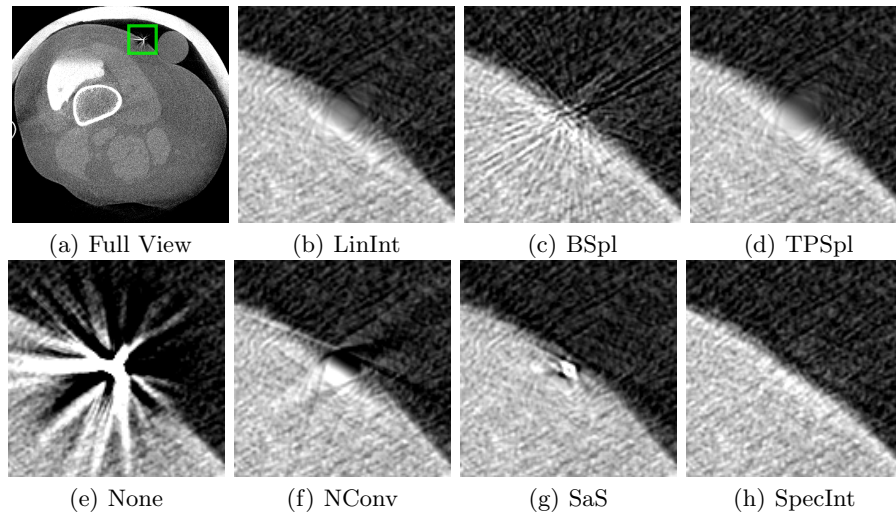


Fig. 2. Bead removal results for the real dataset. Fig. a) shows the full reconstruction. Fig. b) to h) show the method comparison focused on the marked rectangular region.

Acknowledgements

The authors gratefully acknowledge funding of the Research Training Group 1773 “Heterogeneous Image Systems” and the Erlangen Graduate School in Advanced Optical Technologies (SAOT) by the German Research Foundation (DFG).

References

1. Mitrovic U, Spiclin Z, Likar B, Pernus F. 3D-2D Registration of Cerebral Angiograms: A Method and Evaluation on Clinical Images. *Medical Imaging, IEEE Transactions on*. 2013;32(8):1550–1563.
2. Aach T, Metzler VH. Defect interpolation in digital radiography: how object-oriented transform coding helps. In: *Proc. SPIE*. vol. 4322; 2001. p. 824–835.
3. Schwemmer C, Prümmer M, Daum V, Hornegger J. High-Density Object Removal from Projection Images using Low-Frequency-Based Object Masking. In: *Bildverarbeitung für die Medizin 2010 - Algorithmen - Systeme - Anwendungen*. Informatik aktuell. Berlin; 2010. p. 365–369.
4. Loy G, Zelinsky A. Fast radial symmetry for detecting points of interest. *Pattern Analysis and Machine Intelligence, IEEE Transactions on*. 2003;25(8):959–973.
5. Kapur J, Sahoo PK, Wong A. A new method for gray-level picture thresholding using the entropy of the histogram. *Computer vision, graphics, and image processing*. 1985;29(3):273–285.
6. Marchant TE, Amer AM, Moore CJ. Measurement of inter and intra fraction organ motion in radiotherapy using cone beam CT projection images. *Physics in Medicine and Biology*. 2008;53(4):1087.
7. Knutsson H, Westin CF. Normalized and Differential Convolution: Methods for Interpolation and Filtering of Incomplete and Uncertain data. In: *Proceedings of Computer Vision and Pattern Recognition ('93)*; 1993. p. 515–523.